European Journal of Chemistry

Check for updates

View Journal Online
View Article Online

Detailed analytical studies of 1,2,4-triazole derivatized quinoline

Shilpa Mallappa Somagond [1], Manjunath Ningappa Wari [2], Saba Kauser Jaweed Shaikh [1], Sanjeev Ramchandra Inamdar [2], Madan Kumar Shankar [3], Dasappa Jagadeesh Prasad [4] and Ravindra Ramappa Kamble [1,*]

[1] *Department of Chemistry, Karnatak University, Dharwad, Karnataka 580003, India*
shilpasomagond@gmail.com (S.M.S.), saba9805@gmail.com (S.K.J.S.), kamchem9@gmail.com (R.R.K.)
[2] *Department of Physics, Karnatak University Dharwad, Karnataka 580003, India*
sm5wari@gmail.com (M.N.W.), him_lax3@yahoo.com (S.R.I.)
[3] *Department of Science and Technology, PURSE Laboratory, Mangalore University, Mangalagangothri, Karnataka 574199, India*
madan.mx@gmail.com (M.K.S.)
[4] *Department of Chemistry, Mangalore University, Konaje, Mangalore, Karnataka 574199, India*
jprasad2003@gmail.com (D.J.P.)

* *Corresponding author at: Department of Chemistry, Karnatak University, Dharwad, Karnataka 580003, India.*
Tel: +91.836.2445998 Fax: +91.836.2747884 e-mail: kamchem9@gmail.com (R.R. Kamble).

RESEARCH ARTICLE

10.5155/eurjchem.10.4.281-294.1844

Received: 07 March 2019
Received in revised form: 25 July 2019
Accepted: 30 July 2019
Published online: 31 December 2019
Printed: 31 December 2019

KEYWORDS

UV absorption
Hirshfeld surface
Cyclic voltammetry
Single crystal structure
Natural bond orbital (NBO)
Time Dependent-Density Functional Theory

ABSTRACT

The present study describes, the X-ray single crystal analysis of 4-((2-chloro-6-methoxyquinolin-3-yl)methyl)-2-phenyl-2*H*-1,2,4-triazol-3(4*H*)-one (TMQ). The crystal data for $C_{19}H_{15}ClN_4O_2$: monoclinic, space group $P2_1/n$ (no. 14), a = 7.3314(15) Å, b = 12.459(3) Å, c = 18.948(4) Å, β = 98.322(9)°, V = 1712.5(6) Å^3, Z = 4, T = 296.15 K, μ(MoKα) = 0.245 mm^{-1}, *Dcalc* = 1.423 g/cm^3, 5082 reflections measured (3.926° ≤ 2Θ ≤ 38.556°), 1428 unique (R_{int} = 0.0545, R_{sigma} = 0.0574) which were used in all calculations. The final R_1 was 0.0423 (I >2σ(I)) and wR_2 was 0.1145 (all data). The Density functional theory optimized molecular geometries in TMQ agree closely with those obtained from crystallographic studies. The Highest Occupied Molecular Orbital (HOMO) and Lowest Unoccupied Molecular Orbital (LUMO) energy levels and energy gap were calculated by experimental (UV absorption & Cyclic voltammetry) and theoretical studies in two different solvents. The natural bond orbital analysis was performed to understand the molecular interaction on the basis of stability of molecule arising from hyper-conjugative interaction and charge delocalization. Hirshfeld surface and their related fingerprint plots enabled the identification of significant intermolecular interaction. The molecular electrostatic potential analysis provides the visual image of the chemically active sites and comparable reaction of atoms.

Cite this: *Eur. J. Chem.* **2019**, *10(4)*, 281-294 **Journal website**: www.eurjchem.com

1. Introduction

Quinoline, an aza heterocycle, is pharmaceutically an important class of compound that exists as an emergence of pyridine ring and one benzene ring fused together at nearby two (side) carbon atoms [1]. These are widely used as a source compounds for the synthesis of numerous drugs. Many quinoline based drugs such as Captothecine (anticancer) [2] and Cryptolepine (antimalarial) [3] are available in the market. This skeleton also showed a broad spectrum of biological activities including antiasthmatic [4], antidiabetic [5], antibacterial [6], antitoxoplasma [7], antifungal [8] and anti-HIV [9] activities. Due to the presence of nitrogen, the quinoline moieties act as chelating agent as well as a weak base [10]. Some of thequinoline derivatives are often used as fluorescent materials and sensors due to their rigid structure, high fluorescent yield, and large energy gaps [11].

The 1,2,4-triazole scaffolds have attracted significant interest as chemotherapeutic agents, where they possess diverse pharmacological activities [12]. 1,2,4-Triazole nucleus is the main structural motif of many commercially available drugs including Fluconazole, Ribavirin, Letrozole and Itraconazole *etc*. [13-15].

4-((2-Chloro-6-methoxyquinolin-3-yl)methyl)-2-phenyl-2*H*-1,2,4-triazol-3(4*H*)-one (TMQ) was designed and molecular docking study was performed to explore the mechanism of anti-TB as well as anticancer activity and to study the intermolecular interactions between the targeted enzyme (Enoyl-acyl carrier protein) and TMQ. Based on impressive outcome of docking study (C-Score = 5.89) of the TMQ, the molecule was synthesized structure was characterized. Further, *invitro* study was carried out and it was found that this molecule is promising candidate for developing novel anticancer (GI_{50} = 63.15 μM) and anti-tubercular (MIC_{90} = 0.100 μM) agent [16].

http://dx.doi.org/10.5155/eurjchem.10.4.281-294.1844

Table 1. Summary of the crystal structure, data collection, and crystallographic refinement data of TMQ.

Parameter	Values
Empirical formula	$C_{19}H_{15}ClN_4O_2$
Formula weight	366.80
Temperature (K)	296.15
Crystal system	Monoclinic
Space group	$P2_1/n$
a (Å)	7.3314(15)
b (Å)	12.459(3)
c (Å)	18.948(4)
β (°)	98.322(9)
Volume (Å^3)	1712.5(6)
Z	4
ρ_{calc}(g/cm^3)	1.423
μ(mm^{-1})	0.245
F(000)	760.0
Crystal size (mm^3)	0.15 × 0.12 × 0.11
Radiation	MoKα (λ = 0.71073)
2Θ range for data collection (°)	3.926 to 38.556
Index ranges	$-5 \le h \le 6$, $-11 \le k \le 10$, $-17 \le l \le 16$
Reflections collected	5082
Independent reflections	1428 [R_{int} = 0.0545, R_{sigma} = 0.0574]
Data/restraints/parameters	1428/0/236
Goodness-of-fit on F^2	1.021
Final R indexes [I≥2σ (I)]	R_1 = 0.0423, wR_2 = 0.1029
Final R indexes [all data]	R_1 = 0.0588, wR_2 = 0.1145
Largest diff. peak/hole (e.Å^{-3})	0.23/-0.19
CCDC deposition number	1828103

The structural, spectroscopic and photophysical behavior of a molecule depends on function of its overall molecular structure and hence there is a scope in the synthesis of novel conjugate molecules by combining two different moieties together and studying their properties [17]. Also, the spectroscopic and structural behaviors of various molecules using both experimental and theoretical methods have fascinated the curiosity of researchers for many years. Density functional theory (DFT) has become a very useful tool for theoretical calculation in current years. The theoretical calculations using DFT have been utilized to study molecular properties such as structural, spectroscopic and photophysical properties [18-21]. DFT is computationally less challenging than wave function as it also expresses small molecules more reliably than Hartree-Fock theory [22,23].

In the present work, a combined approach by X-ray crystallography (XRD) and DFT calculation was handled, which takes the benefit of both the reliability of the experimental technique and high interpretative influence of the theoretical studies and the accuracy. The structural confirmation was done by XRD data. Since, X-ray diffraction study has become indispensable device in crystal chemistry as it assists in solving the molecular structure, magnitudes and directional characteristics. The exact results of molecular structure of compound TMQ will become important due to experimental facts which help in designing molecules for potential pharmacological property. The theoretical structural predicttions have been carried out by using density functional theory. Ultraviolet (UV)-Visible spectra of TMQ in gaseous phase, ethanol, and acetonitrile are simulated using the Time-dependent density functional theory (TD-DFT). The HOMO and LUMO are analyzed to describe the electronic transition properties of the systems investigated. The theoretically predicted UV Visible spectra of TMQ are compared with the observed experimental results, and discussed. The HOMO and LUMO are also determined by using cyclic voltammetry technique and these are in good agreement with the theoretical results. The general structural features and to predict the reactivity of a molecule, natural bond orbital (NBO) analysis has been carried out which provides important information regarding orbital interactions and electron density among them [24].

2. Experimental

2.1. Synthesis

4-((2-Chloro-6-methoxyquinolin-3-yl)methyl)-2-phenyl-2*H*-1,2,4-triazol-3(4*H*)-one was synthesized according to reported method [16]. TMQwas dissolved in DMSO and heated until the moisture is eliminated. The saturated solution was filtered through the Whatman filter paper into a clean and dry beaker and kept aside for slow evaporation for a period of 15 days at room temperature. Purple colored rectangular shaped crystals of TMQwere collected. Good diffraction quality single crystals were studied further for structural analysis.

2.2. X-ray crystallography

A single crystal of dimensions 0.11 × 0.12 × 0.15 mm of TMQ was chosen for X-ray diffraction study. The X-ray intensity data were collected at a temperature of 293 K on a Rigaku Saturn724 diffractometer using graphite monochromated MoK_α radiation. A complete data set was processed using *CrystalClear* [25]. The structure was solved by direct method and refined by full-matrix least squares method on F^2 using SHELXS and SHELXL programs [26]. All the non-hydrogen atoms were revealed in the first difference Fourier map itself. All the hydrogen atoms were positioned geometrically and refined using a riding model. After ten cycles of refinement, the final difference Fourier map showed peaks of no chemical significance. The geometrical calculations were carried out using the program PLATON [27]. The molecular and packing diagrams were generated using the software MERCURY [28]. The details of the crystal structure and data refinement are given in Table 1. The ORTEP [28] of the molecule with thermal ellipsoids are drawn at 50% probability is shown in Figure 1.

2.3. Hirshfeld surface calculations

Three-dimensional (3D) molecular Hirshfeld surfaces and the two-dimensional (2D) fingerprint plots represent a new way of visualizing and analysing intermolecular interactions in molecular crystals, and are basically different from conventional methods of crystal structure analysis. The molecular Hirshfeld surface [29] in the crystal of organic compounds is created by dividing space in the crystal into regions where the electron distribution as the sum of atoms for the molecule dominates the corresponding sum over the crystal.

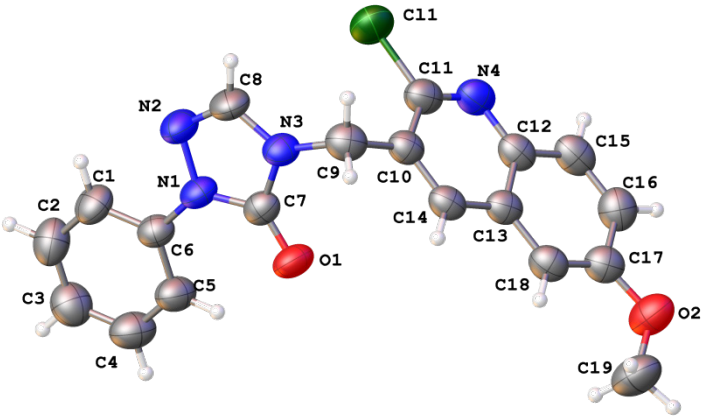

Figure 1. ORTEP of TMQ showing the atomic numbering system. Displacement ellipsoids are drawn with 50% probability.

Hirshfeld surfaces and their related fingerprint plots are generated using the program Crystal Explorer 3.0 [30]. The crystallographic information file (.cif) is given as input to the Crystal Explorer program. The Hirshfeld surface is unique for a given crystal structure and for a set of spherical atomic electron densities. Each point on the Hirshfeld surface is specified with two distances: the distance from the Hirshfeld surface to the nearest nucleus inside the surface is $d_i$and to the nearest nucleus outside the surface is d_e. Then d_{norm} is the normalized contact distance which is defined in terms of d_i, $d_e$and the van der Waals radii (*vdW*) of the atoms. The electrostatic potential is mapped on Hirshfeld surface using STO-3G (Slater-type-orbitals simulated by 3 Gaussians) basis set at the Hartree-Fock theory over the range −0.069 au (red), through 0 (white) to 0.043 au (blue). Crystal geometries were used as input to the TONTO [31] integrated with Crystal Explorer. The acceptor atoms in these interactions are shown with negative electrostatic potentials (red regions) and donor atoms are shown with positive electrostatic potentials (blue regions) [32].

2.4. UV absorption spectroscopy

Absorption spectra of TMQ was recorded using UV-Vis, NIR (JASCO V-670, Japan) spectrophotometer at room temperature, keeping the concentrations of compound 1×10^{-5} M in ethanol and acetonitrile.

2.5. Cyclic voltammetry (CV)

Cyclic voltammetry (CV) study of TMQ was carried out using an Electrochemicalanalyzer / Work station (model 600E series, USA) at room temperature. CV consists of three electrode system that is Ag/AgCl reference electrode (RE), platinum counter electrode (CE) and glassy carbon working electrode (WE). The CV measurements of TMQ (1×10^{-3} M concentration) were obtained at 0.1 M with tetrabutyl ammonium perchlorate as supporting electrolyte in dimethyl-sulphoxide (Acetonitrile) solvent with a scan rate 100 mV/s.

2.6. Density functional theory (DFT) calculations

The DFT calculations were performed using Gaussian 09 software package [33]. The potential energy surface scan has been carried out with (Hartree-Fock) HF/6-31G level to place the molecule at local minima. The geometry at local minima has been assumed as starting point for the calculation by utilizing Becke's three parameter hybrid model with the Lee-Yang-Parr correlation functional (B3LYP) method [34,35]. The geometry is optimized with 6-31++G(d,p) and 6-311++G(2d,p) basis sets for comparison with XRD data. The HOMO (E_{HOMO}), LUMO (E_{LUMO}) energy levels and energy gap (E_g) were calculated by TD-DFT in gas phase and in two different solvents using 6-311++G(2d,p) basis set. The NBO analysis was performed using NBO 3.1 program [36] as implemented in the Gaussian 09 package at the DFT/B3LYP level using 6-311++G(2d,p) basis set.The molecular electrostatic potential surfaces (MEPs) and the Mulliken charge distributions of the title molecule were obtained from the population analysis calculations and visualized using Gauss View 5 [37].

2.7. Molecular electrostatic potential

The molecular electrostatic potential (MEP) surface was determined by DFT level in order to know the relative polarity of the molecule. MEP is formed by the nuclei and the electrons (treated as static distribution of charge) and is typically visualized through its values on the molecular electron density. MEP mapping is very helpful descriptor in understanding sites for relative reactivity towards electrophilic and nucleophilic [38] attacks, in studies of biological identification as well as hydrogen bonding interactions [39,40]. The electrostatic potential V(r) has been mainly useful as sign of the regions or sites of a molecule to which an approaching electrophile is primarily attracted, and is also well matched for analyzing processes based on the "recognition" of one molecule by another, as in enzyme-substrate, drug-receptor, and interactions, since it is through their potentials that the two species initially "see" each other [41,42].

3. Results and discussion

3.1. Description of the crystal structure

The ORTEP of TMQ with thermal ellipsoids are drawn at 50% probability shown in Figure 1. The title molecule crystallizes in monoclinic crystal system (space group $P2_1/n$) with unit cell dimensions a = 7.3314(15) Å, b = 12.459(3) Å, c = 18.948(4) Å, β = 98.322(9)° and Z = 4. Crystallographic data, details of the data collections and structure refinement parameters of the compoundTMQ were determined. The resulted all bond lengths, bond angles and dihedral angles are in good agreement with the calculated values, and tabulated in Tables 2-4, respectively.

Table 2. Experimental and calculated bond lengths (Å) for TMQ.

Atoms	Experimental	Calculated (B3LYP/6-31 ++G(d,p))	Calculated (B3LYP/6-311 ++G(2d,p))
Cl1-Cl1	1.742(4)	1.778	1.778
O2-C19	1.420(5)	1.425	1.422
O2-C17	1.358(5)	1.361	1.358
N4-C11	1.294(5)	1.299	1.291
N4-C12	1.354(4)	1.363	1.359
O1-C7	1.215(4)	1.229	1.220
N1-N2	1.395(4)	1.387	1.385
N1-C7	1.374(5)	1.389	1.386
N1-C6	1.412(5)	1.422	1.418
N2-C8	1.275(4)	1.298	1.291
C17-C18	1.360(5)	1.383	1.376
C17-C16	1.403(5)	1.425	1.420
C18-C13	1.407(5)	1.422	1.416
C13-C14	1.401(5)	1.417	1.411
C13-C12	1.411(5)	1.427	1.421
C14-C10	1.358(5)	1.382	1.375
C10-C9	1.502(5)	1.515	1.511
C10-C11	1.410(5)	1.426	1.420
C9-N3	1.452(4)	1.463	1.460
N3-C7	1.372(4)	1.398	1.395
N3-C8	1.355(4)	1.372	1.367
C6-C5	1.367(5)	1.403	1.397
C6-C1	1.379(5)	1.402	1.396
C5-C4	1.379(5)	1.397	1.390
C4-C3	1.362(5)	1.396	1.389
C3-C2	1.361(5)	1.398	1.391
C12-C15	1.408(5)	1.422	1.416
C15-C16	1.354(5)	1.372	1.365
C2-C1	1.375(5)	1.394	1.388

Table 3. Experimental and calculated bond angles (°) for TMQ.

Atoms	Experimental	Calculated (B3LYP/6-31 ++G(d,p))	Calculated (B3LYP/6-311 ++G(2d,p))
C17-O2-C19	116.8(3)	118.491	118.275
C11-N4-C12	117.5(4)	118.555	118.630
N2-N1-C6	119.1(4)	120.009	120.134
C7-N1-N2	111.3(3)	111.745	111.594
C7-N1-C6	129.4(4)	128.243	128.271
C8-N2-N1	104.0(3)	105.004	105.087
O2-C17-C18	125.6(4)	125.123	125.192
O2-C17-C16	114.4(4)	114.486	114.519
C18-C17-C16	119.9(4)	120.391	120.288
C17-C18-C13	119.9(4)	119.545	119.611
C18-C13-C12	120.3(4)	120.063	120.041
C14-C13-C18	122.3(4)	122.972	122.968
C14-C13-C12	117.4(4)	116.966	116.990
C10-C14-C13	120.8(4)	121.064	121.060
C14-C10-C9	120.5(4)	120.246	120.289
C14-C10-C11	116.3(4)	116.026	116.051
C11-C10-C9	123.2(4)	123.724	123.657
N3-C9-C10	113.6(3)	113.281	113.484
C7-N3-C9	123.0(4)	122.496	122.555
C8-N3-C9	129.2(4)	129.702	129.630
C8-N3-C7	107.8(4)	107.794	107.803
O1-C7-N1	128.6(4)	130.655	130.712
O1-C7-N3	128.1(4)	126.309	126.286
N3-C7-N1	103.4(4)	103.035	103.000
C5-C6-N1	120.6(4)	120.736	120.797
C5-C6-C1	120.1(4)	120.352	120.169
C1-C6-N1	119.3(4)	118.912	119.033
C6-C5-C4	119.2(4)	119.151	119.262
C3-C4-C5	120.6(4)	121.026	121.005
C2-C3-C4	120.3(4)	119.213	119.217
N4-C11-Cl1	115.4(4)	115.611	115.700
N4-C11-C10	126.0(4)	125.473	125.470
C10-C11-Cl1	118.6(4)	118.915	118.827
N4-C12-C13	122.1(4)	121.912	121.791
N4-C12-C15	119.9(4)	119.152	119.304
C15-C12-C13	118.0(4)	118.936	118.904
C16-C15-C12	120.6(4)	120.273	120.279
C15-C16-C17	121.1(4)	120.792	120.874
N2-C8-N3	113.5(4)	112.417	112.512
C3-C2-C1	119.9(4)	120.728	120.711
C2-C1-C6	120.0(4)	119.530	119.634

The Cg1: N1/N2/C8/N3/C7 makes dihedral angles of 78.1(2) and 77.54(18)° with Cg3:C1-C6 and Cg5:N4/C11/C10/C14/C13/C18/C17/C16/C15/C12, respectively. The dihedral angle between Cg3 and Cg5 is 81.31(17)°. In the crystal structure (Table 5 and Figure 2), the intermolecular hydrogen bonds (C(8)-H(8)···O(1)) and intermolecular interaction of the type C(9)-H(9A)[1] → Cg(3) are observed and also intramolecular hydrogen bonds (Table 5) of the type C-H···N and C-H···O are viewed.

Table 4. Experimental and calculated dihedral angles (°).

Atoms	Experimental	Calculated (B3LYP/6-31 ++G(d,p))	Calculated (B3LYP/6-311 ++G(2d,p))
O2-C17-C18-C13	178.8(3)	-179.74	-179.7641
N1-N2-C8-N3	0.7(4)	-0.2628	-0.221
N2-N1-C6-C1	-4.5(5)	0.61318	0.8157
N2-N1-C6-C5	175.5(3)	-179.27	-179.9411
N2-N1-C7-O1	178.6(4)	-179.83	-179.9411
N2-N1-C7-N3	-1.1(4)	0.40339	0.3116
N3-C9-C10-C11	72.1(4)	93.382	93.1891
N3-C9-C10-C14	-108.8(4)	-85.798	-86.4007
N4-C12-C13-C14	-1.1(5)	-0.3902	-0.4741
N4-C12-C13-C18	-179.9(3)	179.709	179.6304
N4-C12-C15-C16	178.7(3)	-179.762	-179.7144
C1-C2-C3-C4	0.4(7)	-0.00438	0.0114
C2-C1-C6-N1	-179.6(3)	-179.933	-179.9218
C2-C1-C6-C5	0.4(6)	-0.04305	0.0238
C2-C3-C4-C5	0.0(7)	0.00853	0.0119
C3-C4-C5-C6	-0.2(6)	-0.02968	-0.0169
C4-C5-C6-N1	-180.0(3)	179.935	179.9436
C4-C5-C6-C1	0.0(6)	0.04691	-0.0011
C6-N1-N2-C8	-175.8(3)	179.782	179.8188
C6-N1-C7-O1	-5.9(6)	0.29240	0.1822
C6-N1-C7-N3	174.5(3)	-179.471	-179.5652
C6-C1-C2-C3	-0.6(6)	0.02160	-0.0291
C7-N1-N2-C8	0.2(4)	-0.1035	-0.0694
C7-N1-C6-C1	-179.7(4)	-179.521	-179.3168
C7-N1-C6-C5	0.3(5)	0.5886	0.738
C7-N3-C8-N2	-1.4(5)	0.5289	0.4277
C7-N3-C9-C10	62.9(4)	87.4729	87.0644
C8-N3-C7-O1	-178.2(4)	179.684	179.8111
C8-N3-C7-N1	1.4(4)	-0.5383	-0.4265
C8-N3-C9-C10	-117.4(4)	-91.375	-92.2879
C9-N3-C7-O1	1.5(6)	0.6145	0.3349
C9-N3-C7-N1	-178.8(3)	-179.607	-179.9026
C9-N3-C8-N2	178.8(3)	179.508	179.8543
C9-C10-C11-Cl1	-1.9(5)	0.62079	0.1931
C9-C10-C11-N4	177.4(4)	179.757	179.8796
C9-C10-C14-C13	-178.2(3)	179.259	179.5551
C11-N4-C12-C13	0.4(5)	-0.08046	-0.0464
C11-N4-C12-C15	-179.3(3)	179.878	179.9016
C11-C10-C14-C13	1.0(5)	0.01812	-0.0649
C12-N4-C11-Cl1	-179.6(3)	-179.792	-179.7365
C12-N4-C11-C10	1.1(6)	0.57460	0.5683
C12-C13-C14-C10	0.3(5)	0.40370	0.5128
C12-C13-C18-C17	0.8(5)	0.07475	0.1291
C12-C15-C16-C17	1.7(6)	0.0285	0.0353
C13-C12-C15-C16	-1.1(5)	0.1977	0.235
C14-C10-C11-Cl1	178.9(3)	179.833	179.7988
C14-C10-C11-N4	-1.8(6)	-0.545	-0.5147
C14-C13-C18-C17	-177.9(3)	-179.819	-179.7598
C15-C12-C13-C14	178.6(3)	179.650	179.5777
C15-C12-C13-C18	-0.2(5)	-0.250	-0.3177
C15-C16-C17-O2	179.8(3)	179.702	179.6871
C15-C16-C17-C18	-1.1(6)	-0.2094	-0.2302
C16-C17-C18-C13	-0.1(5)	0.15403	0.1437
C18-C13-C14-C10	179.1(3)	-179.698	-179.595
C19-O2-C17-C16	-172.1(3)	-179.189	-179.1433
C19-O2-C17-C18	8.9(5)	0.71771	0.7693

Table 5. Intermolecular and Intramolecular interactions of TMQ.

D–H···A/Cg	D–H	H···A/Cg	D···A	D–H···A	Symmetry
C(1)-H(1)···N(2)	0.93	2.43	2.767(6)	102	
C(5)-H(5)···O(1)	0.93	2.30	2.934(5)	125	
C(8)-H(8)···O(1)	0.93	2.27	3.180(5)	167	1/2-*x*, 1/2+*y*, 1/2-*z*
C(9)-H(9A)[1] → Cg(3)		2.68	3.499(4)	143	1+*x*, *y*, *z*

3.2. Hirshfeld surface calculations

Hirshfeld surface analysis is a graphical tool for visualization and was carried out to comprehend relative contributions of various molecular contacts to intermolecular interactions in TMQ [43]. The Hirshfeld surface is a drawing of shape engaged by a molecule in the crystal structure and can be constructed from the electron division [44,45]. The 2D (two-dimensional) fingerprint plots [46,47] obtained by Hirshfeld surface analysis can classify each type of intermolecular interactions, and their relative input can be obtained from the area of the surfaces. The 2D fingerprint plots are constructed based on d_e and d_i distances scales, displayed on the graph axes, in which the d_e represents the distance between the Hirshfeld surface and the nearest $atom_{outside}$, while the d_i represents the distance between this surface and the nearest $atom_{inside}$. The crystal structure packing of the $C_{19}H_{15}N_4ClO_2$compound was generated and quantified with Hirshfeld surface analysis and the associated 2D-fingerprint plots using Crystal Explorer package [48] which accepts a crystal structure input file in CIF format.

The 2D fingerprint plot for all the intermolecular interactions are shown in Figure 3. The H···H interactions which show the most significant contribution of 34.6% to the total Hirshfeld surfaces are reflected in the middle of scattered points in the 2D fingerprint plot.

Table 6. Percentage of various intermolecular contacts contributing to Hirshfeld surface.

Intercontacts	Contribution (%)	Intercontacts	Contribution (%)
H···H	34.6	C···C	06.0
C···H/H···C	20.0	C···Cl/Cl···C	01.0
N···H/H···N	12.8	C···N/N···C	02.7
O···H/H···O	11.1	C···O/O···C	00.5
Cl···H/H···Cl	10.5	Cl···O/O···Cl	00.8

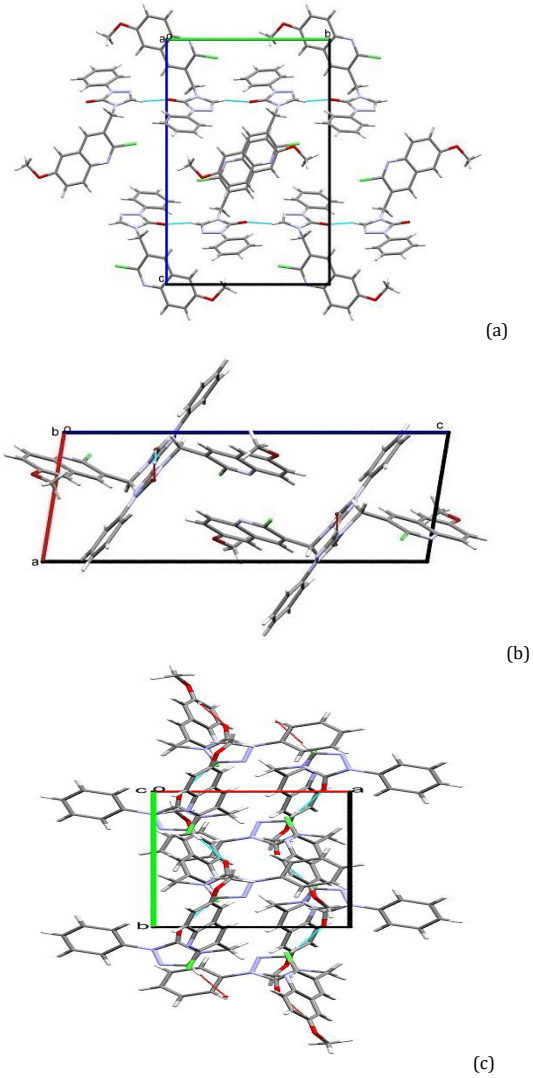

Figure 2. Packing of the molecules viewed along the *a*-(a), *b*-(b) and *c*-axis (c).

The C···H interactions appear as two wings and show a contribution of 20%. The N···H interaction is identified by sharp peaks which comprises 12.8% of the total Hirshfeld surface. The O···H intermolecular contact has covered 11.1% of total Hirshfeld surface area of the molecule apart from that, there aresmaller contributions of Cl…H (10.5%), C···C (6.0%), C···Cl (1.0%), C···N (2.7%), C···O (0.5%), and Cl···O (0.8%) (Table 6). Hence, Hirshfeld surface analysis and fingerprint plots illustrate that the crystal lattice is stabilized by four major interactions H···H, C···H, N···H, and O···H.

In the d_{norm} surface intermolecular contacts relative to the van der Waals radii are represented by method of red-white-blue color scheme where red regions denote shorter contacts with a negative d_{norm} value (higher electron density regions), white regions indicate the distance of contacts exactly comparable to the Van der Waals separation with zero d_{norm} value and blue regions represent longer contacts with a positive d_{norm} value (lower electron density regions) [49]. The large circular deep red colored depressions visible on d_{norm} surfaces indicate hydrogen bonding contacts such asC-H···O and additional spots are due to H-H contacts. The intermolecular interactions are also revealed from the views of electro-static potential mapped over Hirshfeld surface, shown in Figure 4. The acceptor and donor atoms participating in these interactions are shown with respective negative (red regions) and positive electrostatic potentials (blue regions).

3.3. DFT Calculations

The potential energy surface (PES) scan has been carried out on dihedral angles C_1-C_3-C_{12}-H_{14}, C_{30}-N_{35}-C_{12}-H_{14} at HF/6-31G level to examine all possible conformations of the title compound. The PES scan was done by minimizing the potential energy in all geometrical parameters by changing the dihedral angle for 360° rotation for both dihedral angles at steps of every 20°.

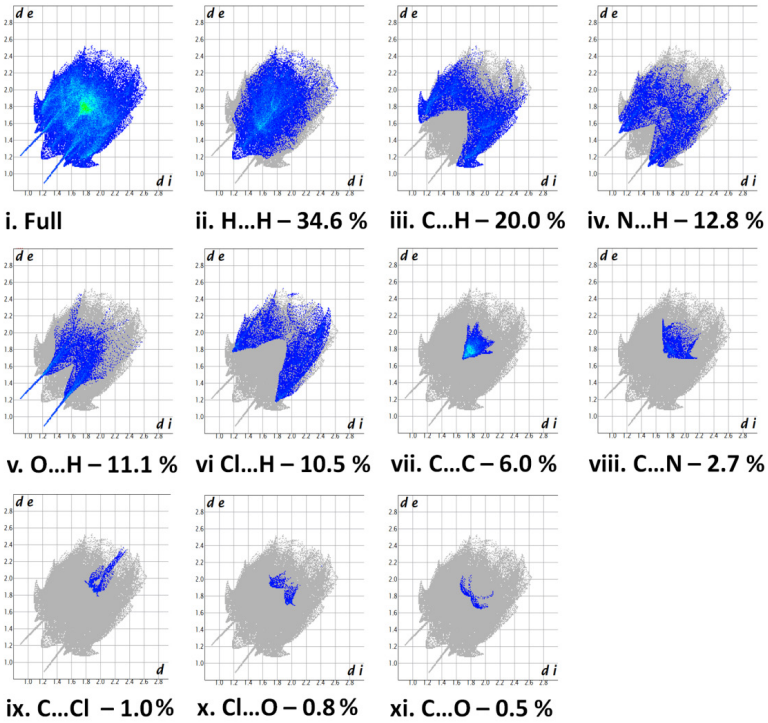

Figure 3. 2D Finger print plots of TMQ.

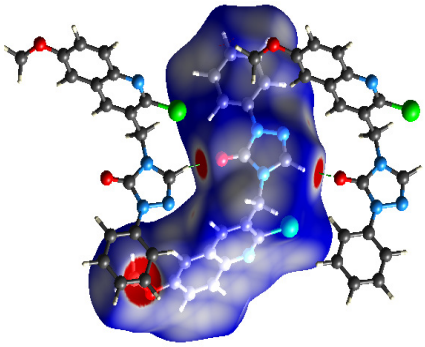

Figure 4. d_{norm} mapped over the Hirshfeld surface with color scale in the range -0.21 au (red) to 1.2 au (blue), green dotted lines show C-H···O intermolecular interaction. The acceptor and donor atoms are shown with respective negative (red) and positive electrostatic potentials (blue).

The geometry of molecule at local minima is selected on the basis of results obtained in PES scan study. The geometry at local minima has been assumed as starting point for the optimization calculation by utilizing Becke's three parameter hybrid model with the Lee-Yang-Parr correlation functional (B3LYP) method. The geometrical parameters (bond lengths, bond angles and dihedral angles) obtained by B3LYP/6-31++G(d,p) and B3LYP/6-31++G(2d,p) methods are compared with experimental results and were found to be reasonably in good agreement with each other (Tables 1-3).

Eventually the theoretical and experimental values differ slightly, as the experimental values of molecule have been recorded in solid phase while theoretical values were computed in gas phase. The optimized structure (Figure 5) from theoretical calculation (DFT) is superimposed with the molecular skeleton from XRD, giving a molecular overlay RMSD value of 0.09 Å (Figure 6). From the obtained results, it is concluded that the B3LYP calculations very well reproduced the geometry of TMQ.

3.4. Molecular electrostatic potential (MEP)

The MEP plot of TMQ (Figure 5) provides a visual image of the chemically active sites and comparative reactivity of atoms. The negative electrostatic potential (red) regions are mainly localized of C=O and C=N group and are promising sites for electrophilic attack. The positive regions (blue) are localized on all the rings, representing possible sites for nucleophilic attack.

3.5. Frontier molecular orbitals

The frontier molecular orbital, the highest occupied molecular orbital (HOMO) and lowest unoccupied molecular orbital (LUMO) are key factors for quantum chemistry and the way of the molecule interacts with other species may be analyzed by knowing the HOMO and LUMO energy values. For organic derivatives, the HOMO-LUMO gap is very important because they relate to specific movements of electrons and may be most significant for single electron transfer.

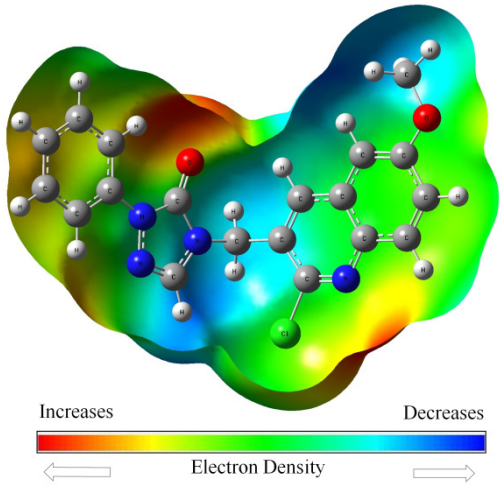

Figure 5. The optimized geometry andMEP plot of TMQ.

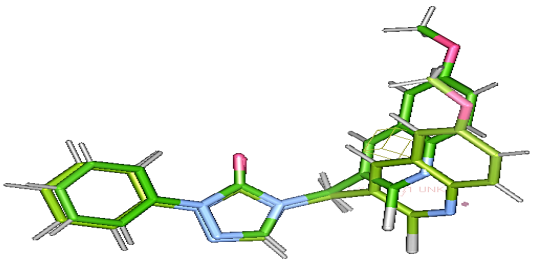

Figure 6. Superimposition diagram TMQ, experimental (Yellow stick model) and theoretical (Green stick model).

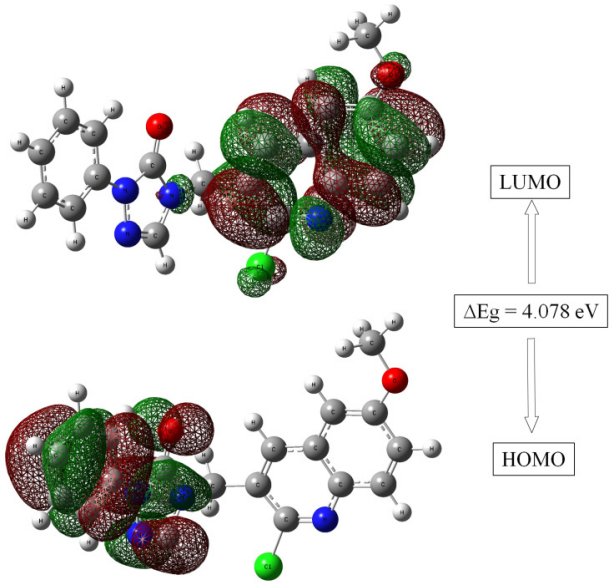

Figure 7. The molecular orbitals and energies for the HOMO and LUMO of TMQ.

The value of HOMO, LUMO and HOMO-LUMO energy gap for the TMQ was calculated by DFT/B3LYP method with 6-311++G(2d,p) basis set. The electron density plots of the HOMO and LUMO for the title molecule is presented in Figure 7. As can be seen from Figure 7 of TMQ, the HOMO is delocalized over the triazole and phenyl ring and LUMO localized over quinoline moiety.The energy values of the highest occupied molecular orbital (HOMO) and lowest unoccupied molecular orbital (LUMO) of TMQ are about -6.164 and -2.086 eV, respectively. In the present study, calculated ($Eg = E_{HOMO}-E_{LUMO}$) energy gap is found to be 4.078 eVwhich shows that there is a transfer of electrons from HOMO to LUMO. Accordingly, the HOMO–LUMO transition implied an electron density transfer from the triazole to quinoline.

3.6. Electronic absorption spectra

Figure 8 showed the experimental absorption spectra of the compound TMQ.

Table 7. Experimental and calculated absorption wavelength λ (nm), excitation energies *E* (eV), and oscillator strengths (*f*) of TMQ calculated by the B3LYP method using 6-311++G(2d,p)basis set.

Experimental method		TD-DFT B3LYP/6-311++G (2d,p)								
Ethanol	Acetonitrile	Gas			Ethanol			Acetonitrile		
λ (nm) Abs.	λ (nm) Abs.	λ (nm)	E (eV)	f	λ (nm)	E (eV)	f	λ (nm)	E (eV)	f
241	252	343.11	3.6135	0.0026	325.60	3.8079	0.0193	326.87	3.7931	0.0273
327	336	318.73	3.8900	0.0676	322.65	3.8427	0.0731	324.43	3.8216	0.0639
		280.85	4.4146	0.0156	282.94	4.3820	0.0193	284.24	4.3619	0.0196
		272.70	4.5465	0.0046	264.69	4.6842	0.0194	265.91	4.6626	0.0175
		271.24	4.5710	0.0252	261.90	4.7340	0.2104	262.92	4.7156	0.2116
		268.52	4.6173	0.0004	257.35	4.8178	0.1212	258.39	4.7983	0.0977
HOMO			-6.3820			-6.3571			-6.1443	
LUMO			-2.1075			-2.0686			-2.0530	
Energy gap			4.2745			4.2885			4.0913	

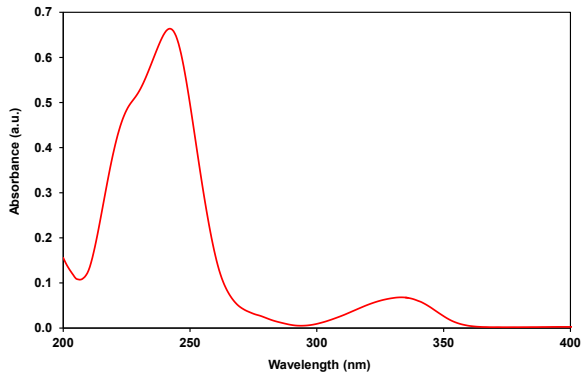

(a)

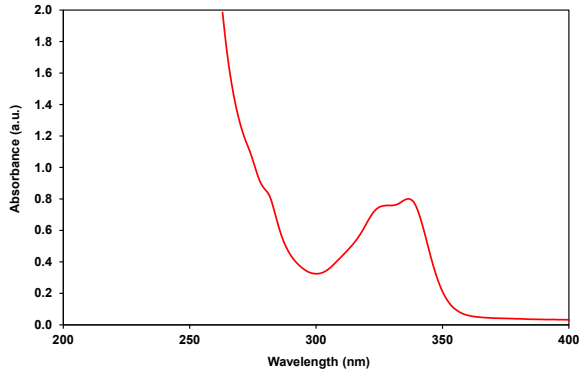

(b)

Figure 8. Experimental electronic absorption spectra of TMQ (1×10^{-5} M) in ethanol (a) and acetonitrile (b) at room temperature.

From Figure 8 maximum absorption wavelength bands were observed at 241, 327 nm in ethanol and 252, 336 nm in acetonitrile for the compound TMQ.

3.6.1. The theoretical electronic absorption spectrum of TMQ

In the UV absorption region, six absorptions at 343.11 nm (λ_1), 318.73 nm (λ_2), 280.85 nm (λ_3) 272.70 nm (λ_4), 271.24 nm (λ_5), and 268.52 nm (λ_6) were observed for the gas phase (Table 7). The oscillator strength (*f*) values corresponding to six wavelengths were 0.0026, 0.0676, 0.0156, 0.0046, 0.0252, 0.0004 oscillator strength value. In the ethanol environment, TMQ exhibited the following six wavelengths at 325.60, nm (λ_1), 322.65 nm (λ_2), 282.94 nm (λ_3), 264.69, nm (λ_4), 261.90 nm (λ_5), and 257.35 nm (λ_6), and the parallel oscillator strength (f) values were observed to be 0.0193, 0.0731, 0.0193, 0.0194, 0.2104, 0.1212, respectively. Acetonitrile environment of TMQ was absorbed at 326.87 nm (λ_1), 324.43 nm (λ_2), 284.24 nm (λ_3), 265.91 nm (λ_4), 262.92 nm (λ_5), and 258.39 nm (λ_6), and the equivalent oscillator strength (*f*) values were observed to be 0.0273, 0.0639, 0.0196, 0.0175, 0.2116, 0.0977.

3.7. Cyclic voltammetry (CV)

In order to investigate the electrochemical properties (HOMO and LUMO) of TMQ, cyclic voltammetry (CV) measurements were carried out. Figure 9 shows cyclic voltammogram of TMQ. HOMO (highest occupied molecular orbital) and LUMO (lowest unoccupied molecular orbital) energy levels were calculated by using the Equations (2) and (3), respectively [50-52] and given in Table 8.

$$E_g = 1240/\lambda \quad (1)$$

$$\text{HOMO} = -[4.44+E^{OX}_{onset}]\ (\text{eV}) \quad (2)$$

$$\text{LUMO} = [\text{HOMO} + E_{Opt}]\ (\text{eV}) \quad (3)$$

where, E^{OX}_{onset} and E_{Opt} are onset oxidation potential and optical band gap respectively. The HOMO energy levels of TMQwas determined and found to be in the range -5.052 eV (v/s. Ag/AgCl).

Table 8. Optical and electrochemical properties of TMQ.

Compound	E_{Opt}/λ_{Onset}(eV/nm)	E^{ox}_{onset} (V)	HOMO (eV) (Expt.)	LUMO (eV) (Expt.)
TMQ	3.512/(353)	0.612	-5.052	-1.54

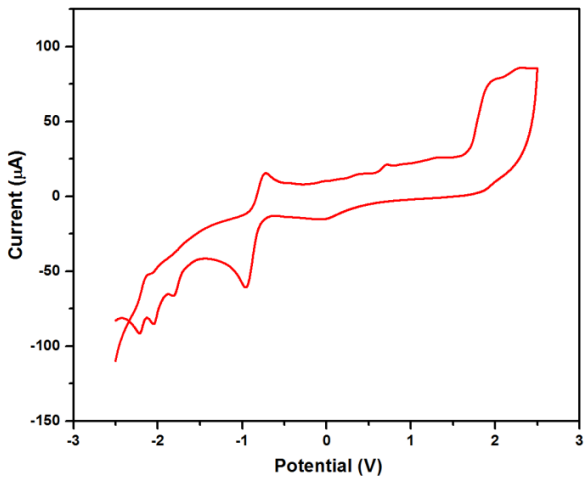

Figure 9. Cyclic voltammogram of TMQ in acetonitrile in the presence of tetrabutylammoniumhexafluorophosphate (Supporting electrolyte) at a scan rate of 100 mV/s.

From Tables 7 and 8, it was observed that the band gaps, HOMO and LUMO values obtained experimentally are approximately in close agreement with values obtained using DFT.

3.8. Mulliken atomic charges and natural charges

The calculation of atomic charges plays a vital role in the application of quantum mechanical calculations to molecular systems. Mulliken charges are evaluated by determining the electron population analysis of each atom as defined in the basic functions. The charge distributions calculated by the Mulliken [53] and NBO methods for the equilibrium geometry of TMQ are given in Table 7. Atomic charges particularly that of reactive ones are very important in defining the reactive nature of molecules under study [54]. This analysis was performed at DFT/B3LYP using two methods 6-31++G (d,p) and 6-311G++(2d,p) basis set. All the hydrogen atoms have positive charges, an acceptor atom for the studied molecule. The distribution of charge on the molecule has an important influence on the vibrational spectra.Mulliken atomic charge of the carbon atoms in the neighbourhood of C22, C23 and C36 become more positive, due to surrounded by more electronegative atoms and shows that the natural atomic charges are more sensitive to the changes in the molecular structure than Mulliken's net charges [55]. C14, Cl1, N5, C17 were changed from negative to positive, due to the effect of Cl atom. Besides, C30, C31, C34 positive to negative most possibly due to electro negativity contribution from halogen (Table 9) [54].

Mulliken charges obtained by different basis sets have been compared and represented in Table 9 in order to examine the sensitivity of the calculated charges to alter in the selection of the basis set. It is interesting to note that change in the charge distribution value is observed with two different basis sets. These natural charge calculations showed the electronegative nature of the O, N and Cl atoms. The carbon (C22) of the triazole C=O group possess the highest positive value of 0.79993 e (6-31++G(d,p)) and 0.78821e (6-311G++ (2d,p)) resulting from its bonding to one electronegative oxygen atom. Of the N-atoms of the triazole ring, the first N-atom has the least negative charge of -0.29196. In addition, all carbon atoms are negatively charged except those attached to the strong electronegative N, O and Cl atom. The oxygen atom attached to aromatic ring (O2) has the lesser negative value -0.53951 e / -0.52973 compared with the O4 (-0.66976 e) [6-31++G (d,p)] / O4 (-0.66559 e) [6-311G++ (2d,p)] attached with the triazole ring. The electropositive nature of all the hydrogen atoms was observed. The nitrogen atom (N3) present in the quinoline ring system possesses more electronegative value -0.45714 and -0.43291.

3.9. NBO analysis

Natural bond orbital (NBO) analysis provides the most precise possible 'natural Lewis structure' by utilizing details of all orbital that are mathematically chosen to consist of the highest probable percentage of the electron density (ED). NBO analysis helps us to understand the delocalization of electron density from 'Lewis occupied donor' NBOs to properly unoccupied 'non-Lewis acceptor' NBOs in the molecule. To explore the intra and inter-molecular interactions, the stabilization energies TMQ were calculated by using second-order perturbation theory. For each donor NBO (i) and acceptor NBO (j), the stabilization energy $E^{(2)}$ associated with electron delocalization between donor and acceptor is calculated as [56].

$$E^{(2)} = \Delta E_{ij} = q_i \frac{F(i,j)^2}{e_j - e_i} \quad (4)$$

Where, q_i → donor orbital occupancy, E_i, E_j → diagonal elements (orbital energies) and F(i,j) → the off-diagonal NBO Fock matrix element. The complete NBO analysis and second order Fock matrix perturbation theory analysis was carried for the title molecule under study using B3LYP/6-311++G(2d,p) level of theory. In NBO analysis, the greater the $E^{(2)}$ (stabilization energy) value, the more exhaustive is the interacttion between electron-donors and electron-acceptors i.e. the more donating tendency from electron donors to electron acceptors, and greater the extent of conjugation of the whole system. The stabilization energies [$E^{(2)}$] of the donor-acceptor interactions with more than 5 kcal/mol determined by second order perturbation analysis of Fock matrix of TMQ is reported in the Table 10.

Table 9. Mulliken and natural charges for TMQ.

Atoms	Atomic charges(Mulliken) 6-31++G(d, p)	Natural charges 6-31++G(d, p)	Atomic charges (Mulliken) 6-311++G(2d, p)	Natural charges 6-311++G(2d, p)
Cl1	0.026991	-0.02079	-0.063774	-0.01987
O2	-0.33771	-0.52973	-0.436535	-0.53951
N3	-0.0695	-0.43291	-0.200568	-0.45714
O4	-0.52227	-0.66559	-0.48729	-0.66976
N5	0.30345	-0.28286	0.118766	-0.29196
N6	-0.37689	-0.29664	-0.376311	-0.3006
C7	-0.201	-0.29866	-0.253533	-0.20103
H8	0.165256	0.20343	0.141882	0.171
H9	0.160746	0.22838	0.173438	0.19262
H10	0.167261	0.20492	0.145156	0.17253
C11	-0.34359	0.31909	0.060499	0.33368
C12	-0.21804	-0.28958	-0.371064	-0.2701
H13	0.09385	0.24587	0.166663	0.21371
C14	0.154984	-0.08152	0.535227	-0.08708
C15	0.300682	-0.14415	-0.222587	-0.0684
H16	0.18063	0.2638	0.235302	0.22128
C17	1.282312	-0.11966	0.939888	-0.12958
C18	-0.71334	-0.25643	-0.714541	-0.18742
H19	0.207724	0.27264	0.209468	0.23384
H20	0.198725	0.26297	0.199435	0.22845
N21	-0.32406	-0.47188	-0.032455	-0.47685
C22	-0.03983	0.78821	0.081885	0.79993
C23	-0.56993	0.14635	0.224346	0.15378
C24	0.34095	-0.25375	-0.131644	-0.2239
H25	0.198003	0.27427	0.213608	0.24405
C26	-0.37709	-0.22412	-0.203351	-0.18635
H27	0.118074	0.24002	0.133359	0.20402
C28	-0.23963	-0.24903	-0.366897	-0.21583
H29	0.105848	0.23851	0.121031	0.20374
C30	-0.17956	0.21024	-0.258584	0.22792
C31	-0.62352	0.15616	-0.09016	0.16325
C32	-0.34019	-0.20288	-0.263201	-0.16782
H33	0.15829	0.25759	0.154558	0.22198
C34	0.208713	-0.24031	0.074353	-0.20578
H35	0.147777	0.25651	0.157561	0.221
C36	0.322857	0.21428	0.125576	0.24812
H37	0.176487	0.24649	0.183568	0.21291
C38	0.073646	-0.2246	-0.085895	-0.18702
H39	0.121259	0.24003	0.134879	0.20421
C40	0.088516	-0.24848	-0.162534	-0.21785
H41	0.173131	0.26405	0.190477	0.23191

The orbital energy decreases due to the interaction between the doubly occupied orbitals and the unoccupied orbital, which is a suitable way to interpret the molecular structure in the electronic point of view. Several other types of parameters, such as hybridization, directionality and partial charges, can also be analysed from NBO tool.

The possible intensive interaction among the whole system in title compound, there is an intermolecular hyper-conjugative interaction of N3-C30 from Cl1 of n(Cl1) → π*(N3-C30) which increases the electron density (0.36900 e) and weakens the respective bonds N3-C30 leading to stabilization of 14.45 kJ/mol. Also, there occurs predominant intermolecular hyper-conjugative interaction of C11-C12 from O2 of π(O2) → π*(C11-C12) which increases the electron density (0.32263 e) that weakens the respective bonds C11-C12 leading to stabilization of 32.71 kJ/mol. There occurs an intermolecular hyper-conjugative interaction of C17-C30 with the electron density (0.04824 e) from N3 of σ(N3) → σ*(C17-C30) results in to weakening the respective bonds C17-C30 and leads to stabilization of 11.76 kJ/mol. These probable observed interactions occur as an increase in electron density in the C-C anti-bonding orbital that weakens the respective bonds. In addition another kind of hyper-conjugative interaction of N5-C22 from O4 of π(O4) → σ*(N5–C22) which increases the electron density (0.09490e) that weakens the respective bonds N5-C22 leading to stabilization of 26.76 kJ/mol and a hyper-conjugative interaction of O4-C22 with stabilization energy of 29.65 kJ/mol occurs from N5 of σ(N5) → σ*(O4-C22) which increases the electron density (0.34442 e) that weakens the respective bonds O4-C22. Moreover, there is also intermolecular hyper-conjugative interaction of N5-C22 from N6 of σ(N6) → σ*(N5-C22) which increases the electron density (0.09490 e) that weakens the respective bonds N5–C22 leading to stabilization of 3.5 kJ/mol. Also, there occurs an intermolecular hyper-conjugative interaction of O4-C22 from σ(N21) → σ*(O4-C22) which increases the electron density (0.34442 e) that weakens the respective bonds O4-C22 leading to stabilization of 26.6 kJ/mol. The successful approach of second-order perturbation theory to predict the hyper-conjugative interaction energy is adopted. Electron density delocalization between the occupied Lewis type (bond or lone pair) NBO orbital and formally unoccupied (anti bond or Rydberg) non-Lewis NBO orbital corresponds to a stabilizing donor-acceptor interaction.

The NBO analysis also describes the bonding in terms of the natural hybrid orbital which occupy a higher energy orbital n3Cl1 (-0.33084 a.u.) with considerable p-character (100.0%) and low occupation number (1.92327) and the other n1(Cl1) occupy a lower energy orbital (-0.93632 a.u.) with *p*-character (16.83%) and high occupation number (1.99365). The NBO analysis also describes the bonding in terms of the natural hybrid orbital n2(O2), which occupy a higher energy orbital (-0.33302 a.u.) with considerable *p*-character (100.0%) and high occupation number (1.83506). The NBO analysis also describes the bonding in terms of the natural hybrid orbital n2(O4), which occupy a higher energy orbital (-0.26529 a.u.) with considerable *p*-character (100.0%) and high occupation number (1.83581). n1N5 which occupy a higher energy orbital (-0.28207 a.u.) with considerable p-character (100.0%) and high occupation number (1.60231). n1N21 which occupy a higher energy orbital (-0.28672 a.u.)

Table 10. Second order perturbation theory analysis of Fock matrix in NBO basis corresponding to the intra-molecular bonds of TMQusing B3LYP/6-311++G (2d,p) basis set.

Donor (i)	Type of bond orbital	ED/e Occupancy	Acceptor (j)	Type of bond orbital	ED/e Occupancy	Energy E(2) kcal/mol	E(i)-E(j)a.u. Energy difference	F(i,j)a.u. Polarized energy
N3-C30	σ	1.98627	N3-C31	σ*	0.02423	1.85	1.40	0.046
N3-C30	π	1.81489	C17-C30	σ*	0.04824	2.93	0.96	0.049
O4-C22	σ	1.98927	N5-C22	σ*	0.09490	0.99	0.96	0.028
O4-C22	π	1.98837	N5-N6	σ*	0.02298	0.93	1.21	0.030
N5-N6	σ	1.97933	N5-C23	σ*	0.03683	0.93	1.22	0.030
N5-C22	σ	1.98479	O4-C22	σ*	0.34442	0.68	0.97	0.025
N6-C36	σ	1.98244	N5-C23	σ*	0.03683	3.77	1.28	0.062
C11-C12	σ	1.97760	O2-C7	σ*	0.00935	1.77	0.86	0.035
C11-C12	π	1.73203	C14-C15	σ*	0.02000	0.58	0.51	0.016
C11-C34	σ	1.97116	O2-C7	σ*	0.00935	4.14	0.81	0.052
C14-C15	σ	1.96937	C11-C12	σ*	0.02684	1.74	1.29	0.042
C15-C17	π	1.71676	N3-C30	π*	0.36900	25.19	0.26	0.074
C17-C18	σ	1.97460	N3-C30	σ*	0.02398	2.98	1.24	0.054
C17-C30	σ	1.97742	N3-C30	σ*	0.02398	3.06	1.31	0.057
N21-C36	σ	1.98581	O4-C22	σ*	0.34442	1.38	0.98	0.036
C23-C24	σ	1.97099	N5-N6	σ*	0.02298	6.18	1.02	0.071
C23-C40	σ	1.97250	N5-N6	σ*	0.02298	1.42	1.02	0.034
C31-C32	σ	1.97425	N3-C30	σ*	0.02398	2.65	1.27	0.052
C32-C34	π	1.75559	C11-C12	π*	0.32263	18.81	0.28	0.067
C38-C40	σ	1.97611	N5-C23	σ*	0.03683	4.14	1.08	0.060
C38-C40	π	1.67977	C26-C28	π*	0.33949	18.74	0.29	0.066
LP Cl1	σ	1.99365	N3-C30	σ*	0.02398	0.62	1.51	0.027
LP O2	σ	1.96453	C11-C12	σ*	0.02684	6.99	1.15	0.080
LP N3	σ	1.89208	C17-C30	σ*	0.04824	11.76	0.83	0.090
LP O4	σ	1.97846	N5-C22	σ*	0.09490	2.37	1.10	0.046
LP N5	σ	1.60231	O4-C22	σ*	0.34442	29.65	0.42	0.101
LP N6	σ	1.94352	N5-N6	σ*	0.02298	0.94	0.71	0.023
LP N21	σ	1.61253	O4-C22	σ*	0.34442	26.60	0.42	0.096

Table 11. NBO results showing the formation of Lewis and non-Lewis orbitals.

Donor(i)	ED/e	EDA%	EDB%	NBO	S%	P%
σN3-C30	1.98627	59.54	40.46	0.7716($sp^{1.57}$)N+	38.84	60.84
πN3-C30	1.81489	56.34	43.66	0.7506 ($sp^{1.00}$)N+	0.00	100.0
σO4-C22	1.98927	70.36	29.64	0.8388 ($sp^{8.84}$)O+	10.12	89.49
πO4-C22	1.98837	65.61	34.39	0.8100 ($sp^{2.43}$)O+	29.02	70.50
σN5-N6	1.97933	55.18	44.82	0.7428 ($sp^{2.66}$)N+	27.30	72.59
σN5-C22	1.98479	63.20	36.80	0.7950 ($sp^{1.94}$)N+	33.92	65.96
σN6-C36	1.98244	58.86	41.14	0.7672 ($sp^{1.61}$)N+	38.08	61.44
σC11-C12	1.97760	50.16	49.84	0.7082 ($sp^{1.54}$)C+	39.35	60.59
π C11-C12	1.73203	45.93	54.07	0.6777 ($sp^{1.00}$)C+	0.00	100.0
σC11-C34	1.97116	50.72	49.28	0.7122 ($sp^{1.80}$)C+	35.64	64.29
σC14-C15	1.96937	51.49	48.51	0.7176 ($sp^{2.00}$)C+	33.30	66.63
πC15-C17	1.71676	45.60	54.40	0.6752 ($sp^{1.00}$)C+	0.00	100.0
σC17-C18	1.97460	50.77	49.23	0.7125 ($sp^{2.15}$)C+	31.72	68.22
σC17-C30	1.97742	50.77	49.23	0.7125 ($sp^{2.04}$)C+	32.89	67.03
σN21-C36	1.98581	63.53	36.47	0.7970 ($sp^{1.96}$)N+	33.74	66.14
σC23-C24	1.97099	51.62	48.38	0.7184 ($sp^{1.68}$)C+	37.33	62.62
σC23-C40	1.97250	51.52	48.48	0.7178 ($sp^{1.71}$)C+	36.94	63.00
σC31-C32	1.97425	51.17	48.83	0.7154 ($sp^{1.87}$)C+	34.88	65.06
πC32-C34	1.75559	49.06	50.94	0.7004 ($sp^{1.00}$)C+	0.00	100.00
σC38-C40	1.97611	49.51	50.49	0.7036 ($sp^{1.81}$)C+	35.59	64.29
πC38-C40	1.67977	49.25	50.75	0.7018 ($sp^{1.00}$)C+	0.00	100.0
n1Cl1	1.99365	-	-	$sp^{0.20}$	83.16	16.83
n2Cl1	1.96696	-	-	$sp^{1.00}$	0.52	99.47
n3Cl1	1.92327	-	-	$sp^{1.00}$	0.00	100.00
n1O2	1.96453	-	-	$sp^{1.65}$	37.66	62.20
n2O2	1.83506	-	-	$sp^{1.00}$	0.00	100.0
n1N3	1.89208	-	-	$sp^{2.77}$	26.40	73.25
n1O4	1.97846	-	-	$sp^{0.64}$	60.80	39.11
n2O4	1.83581	-	-	$sp^{1.00}$	0.00	100.00
n1N5	1.60231	-	-	$sp^{1.00}$	0.00	100.00
n1N6	1.94352	-	-	$sp^{1.45}$	40.70	59.07
n1N21	1.61253	-	-	$sp^{1.00}$	0.00	100.00

with considerable p-character (100.0%) and high occupation number (1.61253). Thus, a very close to pure p-type lone pair orbital participates in the electron donation to the n(Cl1) → π*(N3-C30), π(O2) → π*(C11-C12), σ(N3) → σ*(C17-C30), π(O4) → σ*(N5-C22), σ (N5) → σ*(O4-C22), σ(N6) → σ*(N5-C22), σ(N21) → σ*(O4-C22) interactions in the compound. The results are displayed in Table 11.

4. Conclusions

In the present study, the single crystal X-Ray and DFT analysis of TMQ is reported. It is interesting to note that the optimized geometrical (DFT) results are found in good conformity with the obtained single X-ray diffraction results (XRD). MEP predicts the most reactive component in the molecule. The Hirshfeld surfaces and fingerprint plots predicted that TMQ molecule is stabilized by various intermolecular contacts such as H···H, C···C, C···H/ H···C, N···H/H···N, O···H/H···O, Cl···H/H···Cl, C···Cl/Cl···C, C···N/N···C, C···O/O···C, and Cl···O/O···Cl interactions. A complete molecular picture, stability of the molecule arising from hyper-conjugative interaction, charge delocalization and bond length have been investigated by using Natural Bond Orbital (NBO) analysis. Both experimental and theoretical HOMO and LUMO energies

determine the charge transfer within the molecule and the difference between HOMO and LUMO energy has supported the chemical and bioactivity properties of TMQ. Mulliken atomic charge of the carbon atoms in the neighborhood of C22, C23 and C36 become more positive indicating the direction of delocalization and also showed that the natural atomic charges are more sensitive to the changes in the molecular structure than Mulliken's net charges.

Acknowledgements

Authors wish to thank the University Grants commission, New Delhi for providing financial assistants under UGC UPE FAR-I "Antitumor activity: An Integrated Approach" vide F. No. 14-3/2012 (NS/PE). The authors are grateful to University Scientific Instrumentation Centre (USIC), Karnataka University, Dharwad, for single X-ray diffractometer. Authors thank DST-PURSE Lab for single crystal X-ray diffractometer and other facilities, Karnatak Univeristy Dharwad and Mangalore University, Mangalore. Dr. Shilpa M. Somagond acknowledges the UGC, New Delhi for providing fellowship under project UPE FAR-I Program.

Supporting information

CCDC-1828103 contains the supplementary crystallographic data for this paper. These data can be obtained free of charge via https://www.ccdc.cam.ac.uk/structures/, or by e-mailing data_request@ccdc.cam.ac.uk, or by contacting The Cambridge Crystallographic Data Centre, 12 Union Road, Cambridge CB2 1EZ, UK; fax: +44(0)1223-336033.

Disclosure statement

Conflict of interests: The authors declare that they have no conflict of interest.
Author contributions: All authors contributed equally to this work.
Ethical approval: All ethical guidelines have been adhered.
Sample availability: Sample of the compound is available from the author.

Funding

UGC UPE FAR-I "Antitumor activity: An Integrated Approach" vide F. No. 14-3/2012 (NS/PE), University Grants commission (UGC), New Delhi, India.

ORCID

Shilpa Mallappa Somagond
http://orcid.org/0000-0002-0481-3426
ManjunathNingappa Wari
http://orcid.org/0000-0003-0342-1284
Saba Kauser Jaweed Shaikh
http://orcid.org/0000-0001-8839-9498
Sanjeev Ramchandra Inamdar
http://orcid.org/0000-0003-3398-4897
Madan Kumar Shankar
http://orcid.org/0000-0002-7944-1081
Dasappa Jagadeesh Prasad
http://orcid.org/0000-0003-1333-028X
Ravindra Ramappa Kamble
http://orcid.org/0000-0002-0384-655X

References

[1]. Rastelli, E. J.; Truong, N. T.; Coltart, D. M. *Org. Lett.* **2016**, *18*, 5588-5591.
[2]. Kim, S. H.; Kaplan, J. A.; Sun, Y.; Shieh, A.; Sun, H. L.; Croce, C. M.; Parquette, J. R. *Chem. Eur. J.* **2015**, *21*, 101-105.
[3]. Forkuo, A. D.; Ansah, C.; Boadu, K. M.; Boampong, J. N.; Ameyaw, E. O.; Gyan, B. A.; Ofori, M. F. *Malar. J.* **2016**, *15*, 1-12.
[4]. Gaurav, A.; Singh, R. *Med. Chem. Res.* **2014**, *23*, 5008-5030.
[5]. Lee, H. W.; Lee, H. S.; Park, J. H.; Cheong, J. J.; Kwon, H. B.; Kim, K. O.; Song, H. H. *J. Appl. Biol. Chem.* **2015**, *58*, 1-3 .
[6]. Wise, R.; Andrews, J. M.; Edwards, L. J. *Antimicrob. Agents. Chemother.* **1983**, *23*, 559-564.
[7]. Brown, C. E.; Mc Nulty, J.; Bordon, C.; Yolken, R.; Jones-Brando, L. *Org. Biomol. Chem.* **2016**, *14*, 5951-5955.
[8]. Musiol, R.; Serda, M.; Hensel-Bielowka, S.; Polanski, J. *Curr. Med. Chem.* **2010**, *17*, 1960-1973.
[9]. Luo, Z. G.; Zeng, C. C.; Wang, F.; He, H. Q.; Wang, C. X.; Du, H. G.; Hu, L. M. *Chem. Res. Chin. Univ.* **2009**, *25*, 841-845.
[10]. Liu, H.; Dong, Y.; Zhang, B.; Liu, F.; Tan, C.; Tan, Y.; Jiang, Y. *Sensors Sens. Actuator B-Chem.* **2016**, *234*, 616-624.
[11]. Prodi, L.; Bargossi, C.; Montalti, M.; Zaccheroni, N.; Su, N.; Bradshaw, J. S.; Izatt, R. M.; Savage, P. B. *J. Am. Chem. Soc.* **2000**, *122*, 6769-6770.
[12]. El Ashry, E. S. H.; Awad, L. F.; Soliman, S. M.; Moaty, M. N. A. A.; Ghabbour, H. A.; Barakat, A. *J. Mol. Struct.* **2017**, *1146*, 432-440.
[13]. Almasirad, A.; Tabatabai, S. A.; Faizi, M.; Kebriaeezadeh, A.; Mehrabi, N.; Dalvandi, A.; Shafiee, A. *Bioorg. Med. Chem. Lett.* **2004**, *14*, 6057-6059.
[14]. El Akri, K.; Bougrin, K.; Balzarini, J.; Faraj, A.; Benhida, R. *Bioorg. Med. Chem. Lett.* **2007**, *17*, 6656-6659.
[15]. Karthikeyan, M. S.; Holla, B. S.; Kumari, N. S. *Eur. J. Med. Chem.* **2008**, *43*, 309-314.
[16]. Somagond, S. M.; Kamble R. R.; Kattimani, P. P.; Shaikh, S. J.; Dixit, S. R.; Joshi, S. D.; Devarajegowda, H. C. *Chemistry Select* **2018**, *3*, 2004-2016.
[17]. Yang, F.; Zhang, X. L.; Sun, K.; Xiong, M. J.; Xia, P. F.; Cao, Z. J. *Synth. Met.* **2008**, *158*, 988-992.
[18]. Maiti, A.; Svizhenko, A.; Anantram, M. P. *Phys. Rev. Lett.* **2002**, *88*, 1268051-1268054.
[19]. Zhou, D.; Ma, D.; Wang, Y.; Xianchun Liu; Xinhe Bao; *Chem. Phys. Lett.* **2003**, *373*, 46-51.
[20]. Leconte, J.; Markovits, A.; Skalli, M. K.; Minot, C.; Belmajdoub, A. *Surf. Sci.* **2002**, *497*, 194-204.
[21]. Wang, J.; Liu, C.; Fang, Z.; Liu, Y.; Han, Z.; *J. Phys. Chem. B* **2004**, *108*, 1653-1659.
[22]. Koch, W.; Holthausen, M. C. A.; Chemists Guide to Density Functional Theory, Wiley-VCH, Weinheim, New York, Chichester, 2000.
[23]. Parr, R. G.; Yang, W. T.; Density-Functional Theory of Atoms and Molecules, Oxford University Press, New York, 1989.
[24]. Szafran, M.; Komasa, A.; Adamska, E. B. *J. Mol. Struct. Theochem.* **2007**, *827*, 101-107.
[25]. Rigaku, Crystal Clear SM Expert 2. 0 r15. Software for data collection and processing. Rigaku Corporation, Tokyo, Japan. 2011.
[26]. Sheldrick, G. M. *Acta. Cryst. A* **2008**, *64*, 112-122.
[27]. Spek, A. L. *Acta. Cryst. A* **1990**, *46*, C34.
[28]. Macrae, C. F.; Bruno, I. J.; Chisholm, J. A.; Edging-ton, P. R.; McCabe, P.; Pidcock, E.; Rodriguez-Monge, L.; Taylor, R.; van deStreek, J.; Wood, P. A. *J. Appl. Crystallog.* **2008**, *41*, 466-470.
[29]. McKinnon, J. J.; Spackman, M. A.; Mitchell, A. S.; *J. Acta. Crystallogr. B* **2004**, *60*, 627-668.
[30]. Spackman, M. A.; Jayatilaka, D. *Cryst. Engg. Comm.* **2009**, *11*, 19-32.
[31]. Spackman, M. A.; McKinnon, J. *J. Cryst. Eng. Comm.* **2002**, *4*, 378-392.
[32]. Madan, K. S.; Manjunath, B. C.; Lingaraju, G. S.; Abdoh, M. M. M.; Sadashiva, M. P.; Lokanath, N. K. *Crystal. Struct. Theor. Appl.* **2013**, *3*, 124-131.
[33]. Frisch, M. J.; Trucks, G. W.; Schlegel, H. B.; Scuseria, G. E.; Robb, M. A.; Cheeseman, J. R.; Scalmani, G.; Barone, V.; Mennucci, B.; Petersson, G. A.; Nakatsuji, H.; Caricato, M.; Li, X.; Hratchian, H. P.; Izmaylov, A. F.; Bloino, J.; Zheng, G.; Sonnenberg, J. L.; Hada, M.; Ehara, M.; Toyota, K.; Fukuda, R.; Hasegawa, J.; Ishida, M.; Nakajima, T.; Honda, Y.; Kitao, O.; Nakai, H.; Vreven, T.; Montgomery, J. A.; Peralta, J. E.; Ogliaro, F.; Bearpark, M.; Heyd, J. J.; Brothers, E.; Kudin, K. N.; Staroverov, V. N.; Kobayashi, R.; Normand, J.; Raghavachari, K.; Rendell, A.; Burant, J. C.; Iyengar, S. S.; Tomasi, J.; Cossi, M.; Rega, N.; Millam, J. M.; Klene, M.; Knox, J. E.; Cross, J. B.; Bakken, V.; Adamo, C.; Jaramillo, J.; Gomperts, R.; Stratmann, R. E.; Yazyev, O.; Austin, A. J.; Cammi, R.; Pomelli, C.; Ochterski, J. W.; Martin, R. L.; Morokuma, K.; Zakrzewski, V. G; Voth, G. A.; Salvador, P.; Dannenberg, J. J.; Dapprich, S.; Daniels, A. D.; Farkas, O.; Foresman, J. B.; Ortiz, J. V.; Cioslowski, J.; Fox, D. J. Gaussian, Inc., Gaussian 09, Revision B. 01, Wallingford CT, 2010.
[34]. Hartley, D.; Kidd, H. (Eds.), The Agrochemicals Handbook, Royal Society of Chemistry, Unwin Brothers Ltd., Old Woking Surrey, United Kingdom, 1983.
[35]. Gerhartz, W.; Ullmann's Encyclopedia of Industrial Chemistry, 5th ed., VCH Publishers, Deerfield Beach FL, 1985.
[36]. Glendening, E. D.; Reed, A. E.; Carpenter, J. E.; Weinhold, F.; NBO Version 3. 1, Gaussian Inc., Pittsburgh, PA, 2000-2003.
[37]. Dennington, R.; Keith T.; Millam J.; GaussView, Version 5, Semichem Inc., Shawnee Mission KS, 2009.

[38]. Mckinnon, J. J.; Mitchell, A. S.; Spackman, M. A. *Chem. Eur. J.* **1998**, *4,* 2136-2144.
[39]. Spackman, M. A.; Jayatilaka, D. *Cryst. Eng. Comm.* **2009**, *11*, 249-253.
[40]. Hirshfeld, F. L. *Theor. Chim. Acta.* **1977**, *44,* 129-138.
[41]. Spackman, M. A.; Byrom P. G. *Chem. Phys. Lett.* **1997**, *267,* 215-220.
[42]. Rohl, A. L.; Moret, M.; Kaminsky, W.; Claborn, K.; McKinnon, J. J.; Kahr, B. *Cryst. Growth Des.* **2008**, *8,* 4517-4525.
[43]. Wolff S. K.; Grimwood D. J.; McKinnon J. J.; Turner M. J.; Jayatilaka D.; Spackman M. A. Crystal Explorer, the University of Western Australia, Australia, 2012.
[44]. Skovsen, I.; Christensen, M.; Clausen, H. F.; Overgaard, J.; Stiewe, C.; De gupta, T.; Mueller, E.; Spackman, M. A.; Iversen, B. B. *Inorg. Chem.* **2010**, *49,* 9343-9349.
[45]. Xavier, R. J.; Dinesh, P. *Spectrochim. Acta A* **2014**, *118,* 999-1011.
[46]. Scrocco, E.; Tomasi, J. *Adv. Quant. Chem.* **1978**, *103,* 115-193.
[47]. Luque, F. J.; Lopez, J. M.; Orozco, M. *Theor. Chem. Acc.* **2000**, *103,* 343-345.
[48]. Politzer, P.; Murray, J. S.; in: D. L. Beveridge; R. Lavery (Eds.), Theoretical Biochemistry and Molecular Biophysics: A Comprehensive Survey, Protein, Adenine Press, Schenectady, New York, 2, 1991.
[49]. Scrocco, E.; Tomasi, J. *Curr. Chem.* **1973**, *7,* 95-170.
[50]. Prachumrak, N.; Pansay, S.; Namuangruk, S.; Kaewin, T.; Jungsuttiwong S.; Sudyoadsuk; T.; Promarak V. *Eur. J. Org. Chem.* **2013**, *29*, 6619-6623.
[51]. Kotchapadist, P.; Prachumrak, N.; Sunonnam, T.; Namuangruk, S.; Sudyoadsuk, T.; Keawin, T.; Jungsuttiwong, S.; Promarak, V. *Eur. J. Org. Chem.* **2015**, *3*, 496-505.
[52]. Deshapande, N.; Belavagi N. S.; Sunagar M. G.; Gaonkar S.; Pujar G. H.; Wari M. N.; Inamdar S. R.; Khazi I. A. M. *RSC Adv.* **2015**, *5*, 86685-86696.
[53]. Mulliken, R. S. *J. Chem. Phys.* **1955**, *23*, 1833-1840.
[54]. Kose, E.; Atac, A.; Bardak, F. *J. Mol. Struct.* **2018**, *1163*, 147-160.
[55]. Benzon, K. B.; Varghese, H. T.; Yohannan-Panicker, C.; Pradhan, K.; Bipransh, K. T.; Ashis, K. N.; Van-Alsenoy, C. *Spectrochim. Acta A* **2015**, *146,* 307-322.
[56]. Weinhold, F.; Eric, D. Glendening, NBO 6. 0 Program Manual, University of Wisconsin, Madison, Wisconsin 53706, 2013.